Vol. 46, No. 2 (2024) 251-259, DOI: 10.24874/ti.1531.08.23.11

Tribology in Industry

www.tribology.rs

RESEARCH

Comparative Analysis of Wear Behavior of High Entropy Alloy (TiVNbCrAl) and Ti-based Conventional Alloy (TiNbCrCoAl)

Dheyaa F. Kadhim[a,*]

[a]*Department of Mechanical Engineering, University of Thi-Qar, 64001, Iraq.*

Keywords:

Pin on disk tribometer
Tribological performance
High entropy alloys
High-temperature wear behavior

* Corresponding author:

Dheyaa F. Kadhim
E-mail: dheyaa.kadhim@utq.edu.iq

Received: 8 August 2023
Revised: 10 October 2023
Accepted: 1 November 2023

A B S T R A C T

This research examined the relationships between processing, structure, and property at both room temperature and increased temperature for two BCC high entropy alloy (TiVNbCrAl) and Ti-based conventional alloy (TiNbCrCoAl) prepared using standard arc melting. Both alloys have been determined to have the BCC single-phase solid solution structure. To investigate the hardness and tribological behavior and processes at room temperature and above, microindentation and sliding wear experiments were undertaken. Both alloys display comparable friction behavior when sliding at room temperature, with an average steady-state coefficient of friction (COF) of 0.6. When sliding temperatures rise to 302 °C, the average COF for HEA (TiVNbCrAl) has decreased to a lowest value of ~0.4 due to the creation of a persistent tribochemical layer made of Nb and Cr oxides amid the sliding surfaces, which lowers COF. Whereas, COF for Ti-based conventional alloy remains at higher values of ~0.65. Mechanistic wear analyses revealed that the formation of tribofilms with low interfacial shear strength inside the wear tracks was the cause of this. The tribofilms were identified to be mostly constituted by multi-element solid solution oxides, such as Ni2O5, Cr2O3, and NiO2, according to Raman spectroscopy. The Vickers microharness values for Ti-based conventional alloy is about 365±4 HV. Whereas, for high entropy alloy is about 572±12 HV due to the solid solution strengthening.

1. INTRODUCTION

Since the Bronze Age, alloying has been pursued as a way to strengthen metals. Traditionally, a single element is used as the base material, and solute atoms alter stress fields to prevent mobility of dislocation and reinforce the material, however this typically reduces ductility [1]. One of the pertinent difficulties in materials science is the development of innovative alloys with superior mechanical, tribological, and corrosion properties all at once. Over the past 20 years, these techniques have been utilized successfully to the design of novel materials under the theory of high-entropy alloys (HEAs) [2,3]. Alloys with a minimum of five components and component concentrations ranging from 5 to 35 at.% fall under this category of materials. A stable thermodynamically

substitutional solid mixture with the starting bcc, fcc, or hcp structure is a distinctive feature of HEAs [4-7]. Using this method, we can create new alloys that have a Exceptional balance of toughness, elasticity, hardness, and resistance to wear. Outstanding corrosion resistance is ensured by the large concentration of evenly dispersed passive oxide-forming components, such as Cr. These characteristics of HEAs make them superior to conventional iron alloys as materials with multiple uses [8-10].

Wear and friction are significant engineering issues categorized as their reactions to a tribo-system. However, it is critical to manage material wear in order to lower maintenance costs and avoid material failure in service for aero-engine applications. For steady operations and a long lifespan, wear-resistant materials must be created. Because of the lattice distortion effect and high entropy mixing that supplies the alloy strength and inhibits plastic distortion and dislocation developments, high entropy alloys have recently come into use. These alloys and their distinguishing features have attracted research interest [11,12].

Numerous high entropy alloys with promising properties have been developed as of late, including the high strength (BCC) AlCoCrFeNi and NbMoTaV alloys as well as the high wear-resistant Al0.2Co1.5CrFeNi1.5Ti and Co1.5CrFeNi1.5Ti alloys. Additionally, it was noted that the ability to corrode of the multi-component Cu0.5NiAlCoCrFeSi alloy is higher than that of the standard 304-stainless steel [13]. A high-entropy bulk metallic glasses (BMG) that may be plastically deformed at normal temperature includes CuCoNiCrAlFeTiV, FeCrMnNiCo, NbMoTaWV, CoCrFeNiCu, and AlCoCrFeNi [14].

In this study, two TiNbCrCoAl Conventional and TiVNbCrAl high entropy alloys were manufactured. Microstructure, topological and tribological properties were studied. Wear is considered significant occurrence in many mechanical components. However, little data on the tribological nature of TiVNbCrAl high entropy alloy never been reported in the literature to best of our knowledge. Therefore, we conducted hardness and unidirectional sliding wear tests on both conventional and high entropy alloy to examine the wear behavior and friction mechanisms during room and elevated temperatures.

2. EXPERIMENTAL METHODS

Two BCC alloys—a conventional alloy (TiNbCrCoAl) and a high entropy alloy (TiVNbCrAl)— with either V or Co were investigated. By using an arc-melting and casting process, ingots were created. The specimens had been finished and ground using conventional metallographic techniques for microstructural characterisation. Acetone was used to etch the specimens such that tiny precipitates and grain boundaries could be seen. The wear behavior of both alloys was examined using a Falex ISC-200 (Falex corporation) pin on disk tribometer in accordance with ASTM G99 [15]. In laboratory air with a 40% relative humidity, the sliding coefficient of friction was determined at ambient and higher temperatures (102°C and 302°C). The high entropy alloy samples were put to the test by sliding unidirectionally against Si_3N_4 ball counter faces with 3.175 mm and 23 GPa diameter and hardness. For all tests, the sliding speed was 8.5 mm/s, and the standard load was 0.25 N. The Hertzian contact stress was decided to be less than the alloys' yield strength at 0.6 GPa based on these measurements. For all testing, the overal distance of sliding was 200 m. For the sake of reproducibility, at least two measurements were taken for each high entropy alloy. An optical microscope was used to take pictures of the Si3N4 counter faces and the worn surfaces of the high entropy alloy samples after each test. To measure roughness and wear track depths, a stylus profilometer (Veeco Dektak 150 Profilometer) was employed. To obtain the cross sectional worn area, at least seven traces were obtained across each wear track. According to Archard's equation, the wear factor/rate is determined by dividing the eliminated volume loss over the total sliding distance and applied force. The volume removal can be determined by dividing the worn surface's area by the circular wear track's circumference, assuming uniform wear. Using a Rigaku Ultima III X-ray diffractometer with radiation parameters of 30 kV, 20 mA, a Cu K anode, and a scanning speed of 2 degree/minute, crystal structures were found. An FEI-Nova 200 dual beam electron microscopy instrument was used for the analysis of the microstructural development during the frictional procedure and the wear surface. Using a 532 nm laser wavelength, Raman spectrometer was utilized to identify the tribo-chemical phases on the worn surfaces. Using Shimadzu Vickers hardness measuring devices with a load of 9.8 N and an acquisition duration of 10 seconds, room-temperature micro hardness evaluations were made.

3. RESULTS AND DISCUSSION

3.1 Microstructural and structural analysis

Figure 1 displays the Ti-based conventional alloy XRD pattern. As can be seen, a distinct peak of the BCC phase was found at room temperature for typical alloys.

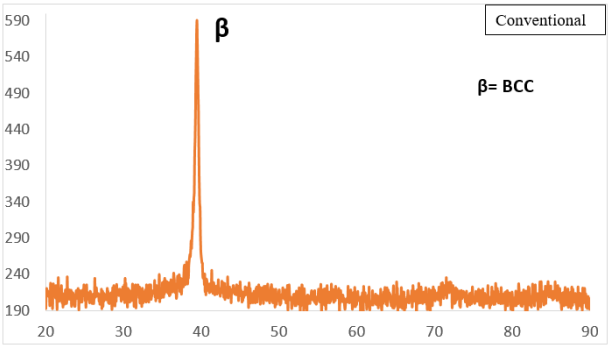

Fig. 1. XRD pattern of Ti-based conventional alloy.

In contrast, one set of peaks that correspond to either a B2 structure or a mixture of the B2 and BCC can be found in the high entropy alloy seen in Figure 2.

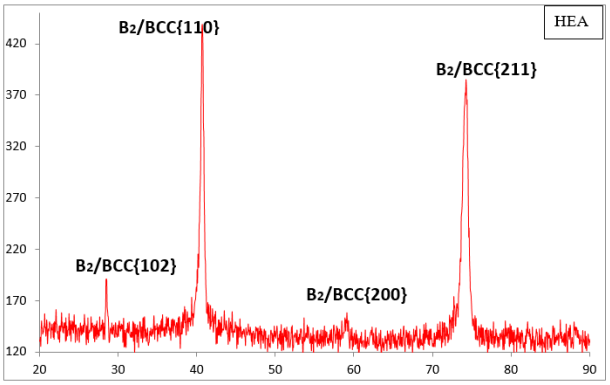

Fig. 2. XRD pattern of high entropy alloy.

In addition, Figure 3 backscattered SEM image shows that both alloys have interdendritic and dendritic morphologies. Table 1 provides the standard alloy chemical ingredients. It should be noticed that Ti predominates in this alloy, followed by Nb. At room temperature, Ti-24Nb-3Al has only one BCC phase, according to Inamura et al [16]. The martensitic phase was discovered to exist in Ti-18Nb-3 Al and Ti-20Nb-3Al alloys at ambient temperature [16]. According to Guo's recommendation, the predicted valence electron concentration (VEC) value for conventional alloy is 4.44, which indicates that the alloy should include a single phase [17], and XRD results are in agreement with this. The chemical compositions for high entropy alloy determined from the EDS data are shown in Table 1. Additionally, the AlNbTiV HEA contains a dendritic BCC phase, according to N.D. Stepanov et al [18]. Nb (24.8 at.%) was abundant in the dendritic sections, while Al (27.6 at.%) enhanced the interdendritic region. The valence electron concentration (VEC), which has been used to determine the phase stability HEAs. VEC is defined by:

$$VEC = \sum_{i=1}^{n} Ci(VEC)i$$

where (VEC)i is the value for contuent elements.

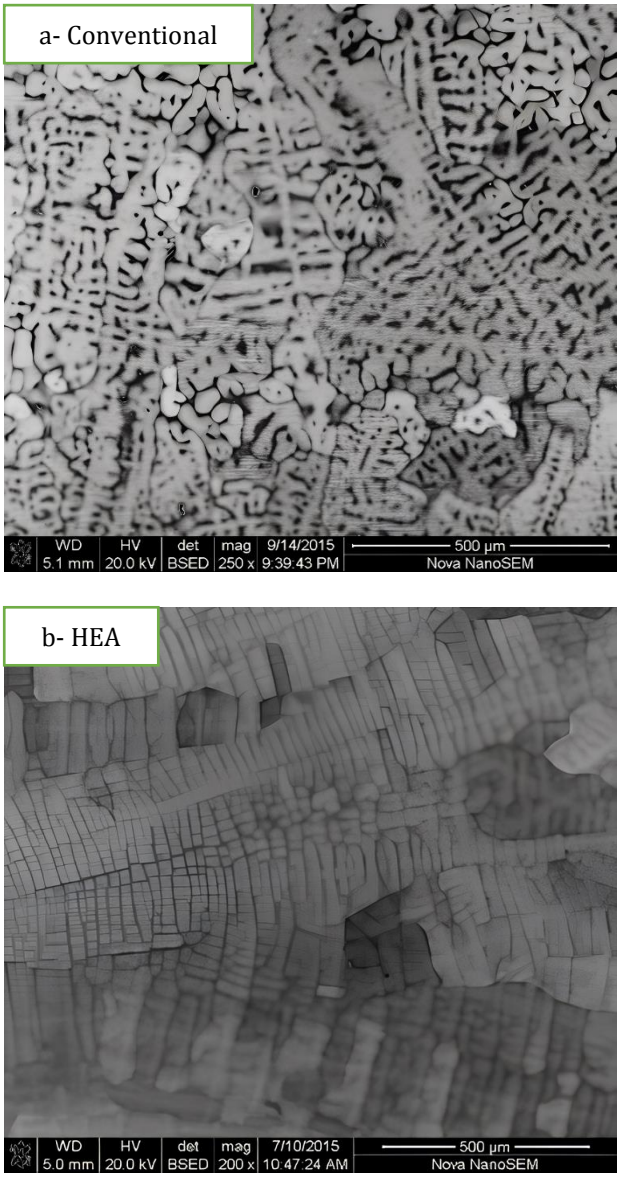

Fig. 3. SEM images of (a) Ti-based conventional and (b) high entropy alloy.

VEC was used to explain why the AlNbTiV HEA produced solid solution instead of intermetallic mixtures. It was discovered that the production of solid solution on the AlNbTiV high entropy alloy requires VEC= 4.25 [18]. Senkov further said that the NbTiZrV alloy has A2 phase. However, BCC and Laves phases were present in CrNbTiVZr and CrNbTiZr alloys [19]. According to Guo's proposal, the multi-component alloy should include a single phase because the estimated VEC value for the alloy is 4.6. [17], and XRD results are in agreement with this. As a result, there is only one BCC solid solution without intermetallics.

Table 1. Composition of Ti-based conventional and high entropy alloy by SEM/EDS performed results.

Alloy	**Element**	Cr	Co	Ti	Nb	Al	V
HEA	At. %	21		18.88	18.68	21.65	20.05
Conventional	At. %	5.2	6.19	68.28	12.46	7.87	

3.2 Micro hardness analysis

The Vickers micro hardness pattern along the surface of both Ti-based conventional alloy and high entropy alloy in the as-cast form is shown in Figure 4.

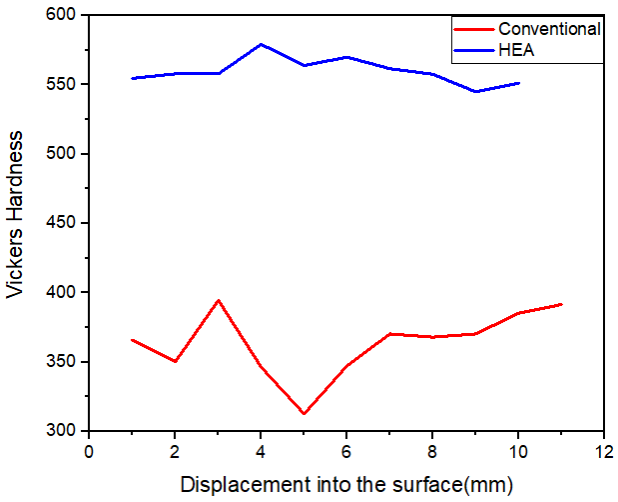

Fig. 4. Microhardness trends of Ti-based conventional and high entropy alloy.

The average hardness value for the conventional alloy 365±4 HV. The high entropy alloy, on the other hand, is made up of almost equiatomic components. The alloy only has one solid BCC solution. Its Vickers hardness is a respectable 572±12 HV. In addition, The high hardness of HEA can be linked to formation of BCC phase which is enhanced by the addition of Ti which considered as bcc stabilizer [20]. Moreover, Al serves to maintain the BCC [21]. The alloy's mechanical attributes are comparable to those of AlNbTiV, which possess microhardness value of 440 HV [18]. Besides, the Al atomic size is considered to be larger than that of other alloy elements. This leads to lattice distortion and promote solid solution strengthening , thus overall HEA strength will be enhanced [22]. Moreover, Vanadium plays a vital role in rising the hardness of HEA as reported by Dong et al [23]. They studied the effect of vanadium on the properties of NiCoAlCrFe HEA. They found that the Vickers harness increased from HV534 to HV648.8 with increasing the vanadium and the solid solution strengthening was the main reason behind the rise in hardness values.

3.3 Wear behavior and tribology properties

3.3.1 Wear behavior at 27°C

Figure 5 shows the friction behaviour of high entropy alloy (TiVNbCrAl) and Ti-based conventional alloy (TiNbCrCoAl) at room temperature. It can be noticed that both alloys behave in similar manner and both alloys had the same value of coefficient of friction (COF) of about ~0.6

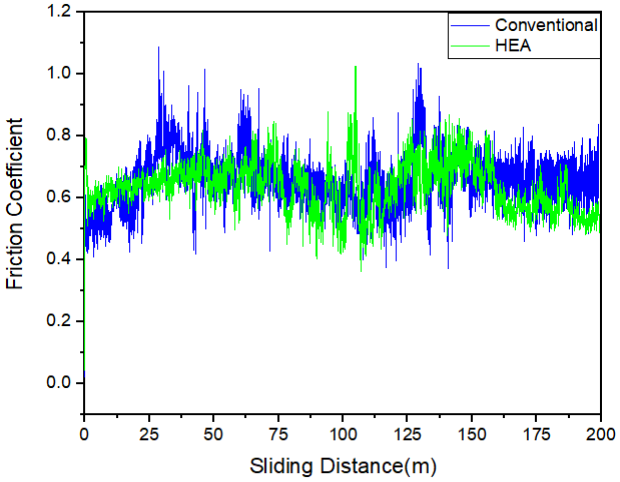

Fig. 5. Friction curve of conventional and high entropy alloy at 27°C.

3.3.2 Wear behavior at 102°C

The friction behavior of Ti-based conventional alloy and HEA at 102°C is shown in Figure 6. In comparison to ambient temperature, the friction is greater. The friction behavior also exhibits a lot of noise. For the Ti-based conventional alloy, the COF increased from ~0.6 to about ~0.8 before reaching steady state. Contrarily, the COF of the high entropy alloy began at 0.8 and decreased through a number of transitions before reaching the steady state COF of ~0.6.

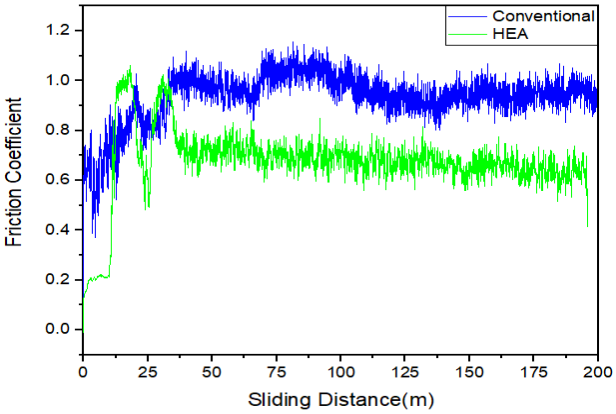

Fig. 6. Friction curve of conventional and high entropy alloy at 102°C.

3.3.3 Wear behavior at 302 °C

Figure 7 depicts the friction behavior of a conventional and high entropy alloy 302°C. The HEA has a steady state COF of roughly ~0.4 due to the presence of Ni and Cr oxides which lowers the friction (which will be discussed later in Raman section). However, the COF of conventional alloy at steady state was roughly~ 0.6.

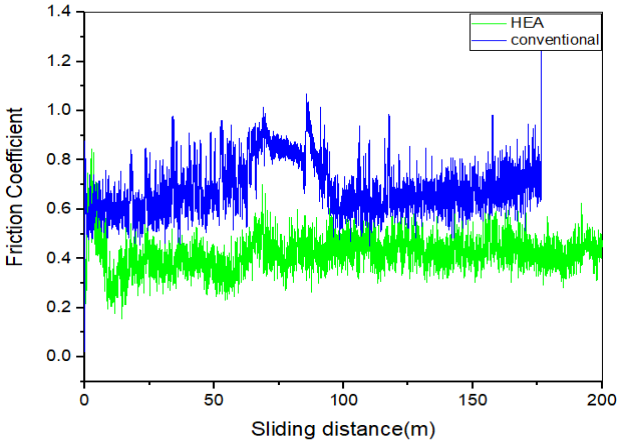

Fig. 7. Friction curve of conventional and high entropy alloy at 302°C.

3.4 Analysis of worn surfaces

3.4.1 Scanning electron microscope of wear scars

According to the morphologies shown in Figures 8 and 9, both alloys suffer from severe abrasive wear, which is evident in the form of plowed grooves and visible plastic deformation.

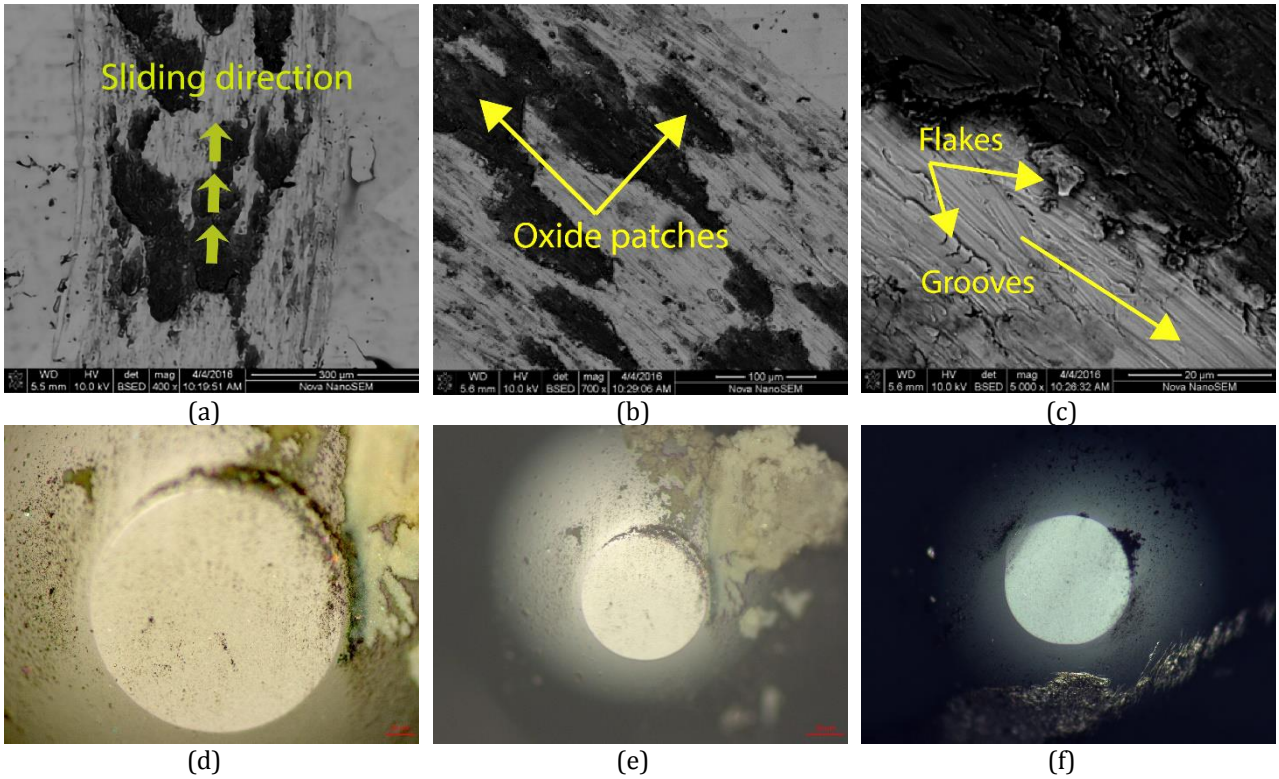

Fig. 8. SEM wear track images of Ti-based conventional alloy (a, b, c) and the corresponding Si3N4 pin surface optical images (d, e, and f).

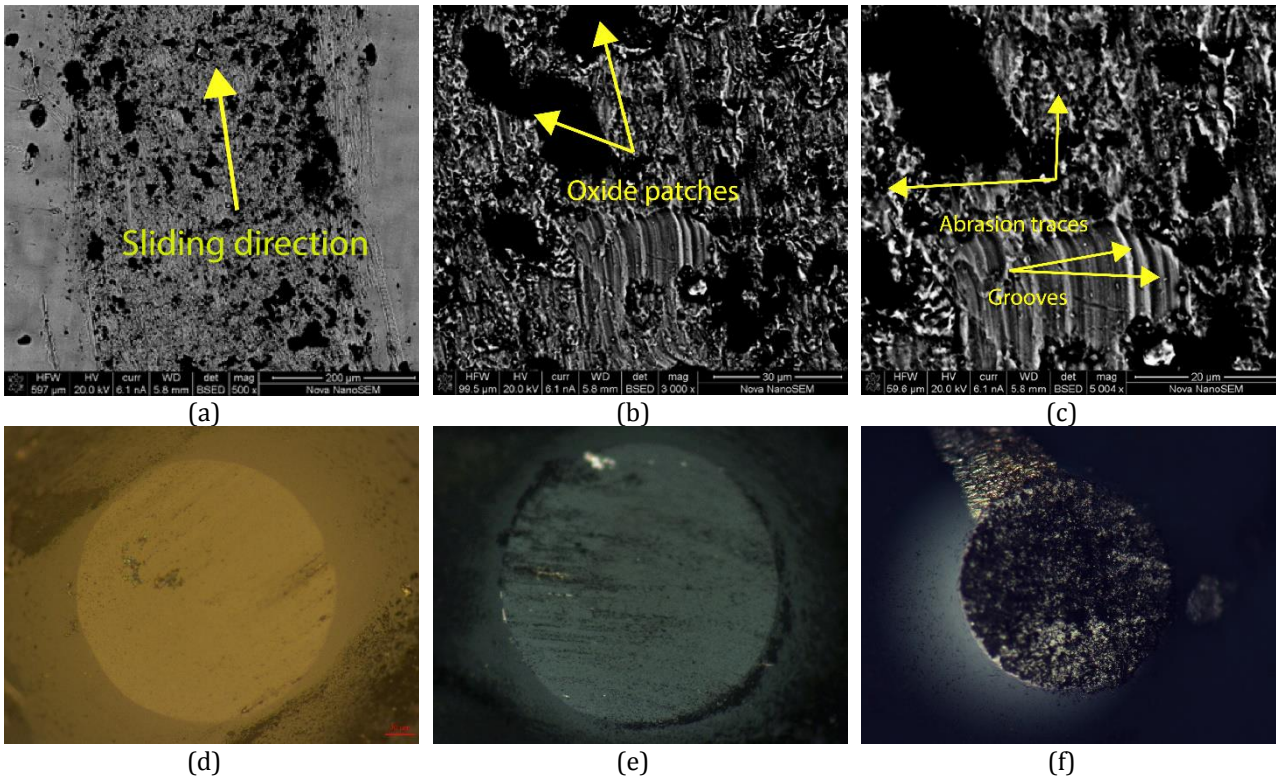

Fig. 9. SEM wear track images of high entropy alloy (a, b, c) and the corresponding Si_3N_4 pin surface optical images (d, e, and f).

The Si_3N_4 counter face's harsh asperities and the consolidated wear detritus seem to have generated the plastic deformation that caused the majority of the material loss in conventional alloy to occur through oxidation wear. However, the oxide particle-induced micro-cutting may also be a factor in the volume loss. Additionally, adhesive wear occurred, as shown by the material transfer and the creation of cracks and oxide spots from delamination. The adhesion theory states [24,25], When two contacting surfaces are moved against one another, The pairing surfaces' irregularities cling to the other side. When sliding, the worn materials will migrate between the two layers. The break off frequently occurs in the softer material. It may be predicted that material is largely transferred from conventional alloy to the $_{Si3N4}$ ball because the hardness of the Si_3N_4 counter face is higher than that of conventional alloy. The surface oxidation of reactive Ti serves as evidence of the presence of oxides at the worn surface [26]. According to the worn scar morphology of the multi-component alloy, the test was conducted under light wear circumstances. Slight adhesive, oxidation, and spalling of the attached material are the main mass removal methods. It may be assumed that during the sliding wear test, volume is transferred from the multi-component alloy to the counter face since the multi-component alloy is softer than the Si_3N_4 counter face [26]. Improved hardness and decreased COF of the multi-component alloy at 102 °C are compatible with the ocular observation of less wear when compared to traditional alloy.

3.4.2 Oxides determination of wear scars

According to the literature-based Raman spectroscopy database [27-32], inside the wear tracks, As illustrated in Figure 10, it can be ascertained that the extremely little wear scars contains a variety of metal oxides, including Nb_2O_5, NbO_2, Cr_2O_3, and TiO_2. According to certain reports [33-34], metal oxides like Cr_2O_3 and Nb_2O_5 can lower the friction coefficient and are effective at preventing alloy fracture . Based on the Raman spectra of the two alloys, it has been determined that the inclusion of NbO_2 and Nb_2O_5 in the high entropy alloy (TiVNbCrAl) wear track also contributes to a reduction in friction and wear as compared to Ti-based conventional alloy (TiNbCrCoAl), which do not contain a large quantities of such tribochemical components.

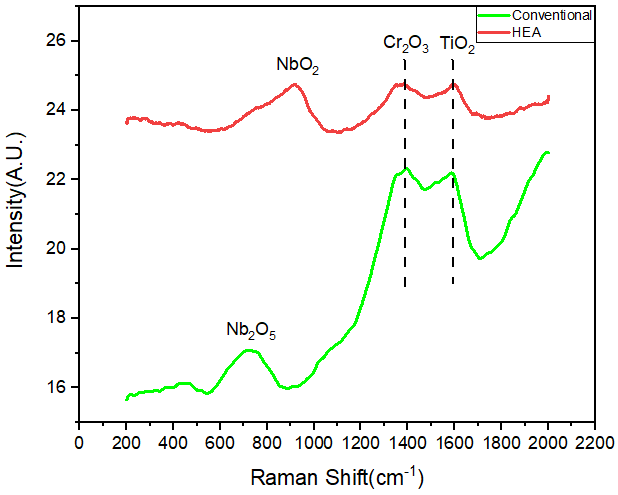

Fig. 10. Raman spectra for Ti-based conventional alloy and high entropy alloy wear tracks at RT.

3.4.3 Calculations of wear rates

The wear rate of HEA and Ti-based conventional alloys were calculated to be 1.12E-07 (mm3/N.m), and 5.55E-08 (mm³/N.m), respectively. The degrees of hardness are respectively 365±4 and 572±12. Intermittent generation of the wear debris is possible. Additionally, the Ti-based conventional alloy, which wears out considerably more quickly than high entropy alloy, has a deep wear track. Nevertheless, the high entropy alloy with the lowest RT friction coefficient has a little greater wear rate. Its slightly decreased hardness is probably to blame for this.

4. CONCLUSION

The as-cast microstructures and wear behaviors of two high entropy alloy (TiVNbCrAl) and Ti-based conventional alloy (TiNbCrCoAl) were investigated. Some important conclusions can be drawn depending on the wear test performed with pin on disk tribometer at room and elevated temperatures.

1. The main phase in Ti-based conventional alloy (TiNbCrCoAl) and high entropy alloy (TiVNbCrAl) is BCC structure.
2. The averaged hardness value for Ti-based conventional alloy is about 365±4 HV. Whereas, for high entropy alloy is about 572±12 HV, that is superior to that of Ti-based conventional alloy. This can be attributed the Presence of Ti and V elements which stabilizes the bcc structure and enhance the Vickers hardness.
3. Ti-based conventional Alloy (TiNbCrCoAl) has wear rate of 1.12E -07 (mm³/N.m), at RT. It demonstrates the worst tribological qualities when combined with increased friction.
4. Due to its relatively ductile BCC solid solution and B2ordered phase, High Entropy Alloy (TiVNbCrAl) has outstanding overall tribological properties at low and high temperatures. The formation of an ongoing tribochemical coating between the sliding surfaces made of Nb and Cr oxides, which helps lower the friction coefficient. Due to its greater Vickers hardness of 57212 HV, it demonstrated a low rate of wear of 5.55 E-08 (mm³/N.m) at RT, outperforming Ti-based Conventional Alloy.

REFERENCES

[1] Y. Zou, H. Ma, and R. Spolenak, "Ultrastrong ductile and stable high-entropy alloys at small scales," *Nature Communications*, vol. 6, no. 1, p. 7748, Jul. 2015, doi: 10.1038/ncomms8748.

[2] D. A. Avila-Salgado, A. Juárez-Hernández, M. Lara Banda, A. Bedolla-Jacuinde, and F. V. Guerra, "Effects of Nb Additions and Heat Treatments on the Microstructure, Hardness and Wear Resistance of CuNiCrSiCoTiNbx High-Entropy Alloys," *Entropy*, vol. 24, no. 9, p. 1195, Aug. 2022, doi: 10.3390/e24091195.

[3] A. Ayyagari, V. Hasannaeimi, H. S. Grewal, H. Arora, and S. Mukherjee, "Corrosion, erosion andwear behavior of complex concentrated alloys: A review," *Metals*, vol. 8, no. 8. Aug. 2018, doi: 10.3390/met8080603.

[4] Y. Yang, X. Luo, T. Ma, L. Wen, L. Hu, and M. Hu, "Effect of Al on characterization and properties of AlxCoCrFeNi high entropy alloy prepared via electro-deoxidization of the metal oxides and vacuum hot pressing sintering process," *Journal of Alloys and Compounds*, vol. 864, p. 158717, Jan. 2021, doi: 10.1016/j.jallcom.2021.158717.

[5] A. Del Ángel-González et al., "Microstructure, Phase Evolution, and Chemical Behavior of CrCuFeNiTiAlx High Entropy Alloys Processed by Mechanical Alloying," *Entropy*, vol. 25, no. 2, p. 256, Jan. 2023, doi: 10.3390/e25020256.

[6] R. R. Eleti, M. Klimova, M. Tikhonovsky, N. Stepanov, and S. Zherebtsov, "Exceptionally high strain-hardening and ductility due to transformation induced plasticity effect in Ti-rich high-entropy alloys," *Scientific Reports*, vol. 10, no. 1, pp. 1–8, Aug. 2020, doi: 10.1038/s41598-020-70298-2.

[7] D. F. Kadhim, M. V Koricherla, and T. W. Scharf, "Room and Elevated Temperature Sliding Friction and Wear Behavior of $Al_{0.3}$CoFeCrNi and $Al_{0.3}$CuFeCrNi$_2$ High Entropy Alloys," *Crystals*, vol. 13, no. 4, p. 609, Apr. 2023, doi: 10.3390/cryst13040609.

[8] S. Mukanov, P. Loginov, A. Fedotov, M. Bychkova, M. Antonyuk, and E. Levashov, "The Effect of Copper on the Microstructure, Wear and Corrosion Resistance of CoCrCuFeNi High-Entropy Alloys Manufactured by Powder Metallurgy," *Materials (Basel)*, vol. 16, no. 3, p. 1178, Jan. 2023, doi: 10.3390/ma16031178.

[9] Z. Yang and C. Jiang, "Surface Characteristic and Friction Behavior of Plasma Sprayed FeCoNiCrMo$_{0.2}$ High Entropy Alloy Coatings on BS960 High-Strength Steel with Subsequent Shot Peening Treatment," *Coatings*, vol. 13, no. 2, P. 303, Jan. 2023, doi: 10.3390/coatings13020303.

[10] L. M. Rymer, T. Lindner, and T. Lampke, "Nb and Mo Influencing the High-Temperature Wear Behavior of HVOF-Sprayed High-Entropy Alloy Coatings," *Coatings*, vol. 13, no. 1, p. 9, Dec. 2022, doi: 10.3390/coatings13010009.

[11] M. Dada, P. Popoola, N. Mathe, and S. Adeosun, "Wear characteristics of laser-deposited AlCoCrCuFeNi high entropy alloy with finite element analysis," *Beni-Suef University Journal of Basic and Applied Sciences*, vol. 11, no. 1, Nov. 2022, doi: 10.1186/s43088-022-00307-y.

[12] D. Zhang, D. Du, G. Liu, Z. Pu, S. Xue, and B. Chang, "Microstructure and Wear Resistance of FeCuNiTiAl High-Entropy Alloy Coating on Ti6Al4V Substrate Fabricated by Laser Metal Deposition," *Lubricants*, vol. 10, no. 10, p. 263, Dec. 2022, doi: 10.3390/lubricants10100263.

[13] P. M. Gopal, K.S. Prakash, V. Kavimani and R. Gopal, "Processing and Properties of AlCoCrFeNi High Entropy Alloys: A Review" *Advances in Materials Science and Engineering*, vol. 2022, pp. 1-13, Oct. 2022, doi: 10.1155/2022/1190161.

[14] Y. Zhang et al., "Microstructures and properties of high-entropy alloys," *Progress in Materials Science*, vol. 61, pp. 1-93, Apr. 2014, doi: 10.1016/j.pmatsci.2013.10.001.

[15] *Standard Test Method for Wear Testing with a Pin-on-Disk*, ASTM G99-95A, 2000.

[16] T. Inamura, Y. Fukui, H. Hosoda, K. Wakashima, and S. Miyazaki, "Relationship between texture and macroscopic transformation strain in severely cold-rolled Ti-Nb-Al superelastic alloy," *Matererials Transactions*, vol. 45, no. 4, pp. 1083–1089, Jan. 2004, doi: 10.2320/matertrans.45.1083.

[17] S. Guo, C. Ng, J. Lu, and C. T. Liu, "Effect of valence electron concentration on stability of fcc or bcc phase in high entropy alloys," *Journal of Applied Physics*, vol. 109, no. 10, May 2011, doi: 10.1063/1.3587228.

[18] N. D. Stepanov, D. G. Shaysultanov, G. A. Salishchev, and M. A. Tikhonovsky, "Structure and mechanical properties of a light-weight AlNbTiV high entropy alloy," *Materials Letters*, vol. 142, pp. 153–155, Mar. 2015, doi: 10.1016/j.matlet.2014.11.162.

[19] O. N. Senkov, S. V. Senkova, C. Woodward, and D. B. Miracle, "Low-density, refractory multi-principal element alloys of the Cr-Nb-Ti-V-Zr system: Microstructure and phase analysis," *Acta Materialia*, vol. 61, no. 5, pp. 1545–1557, Mar. 2013, doi: 10.1016/j.actamat.2012.11.032.

[20] R. Razuan, N. A. Jani, M. K. Harun, and M. K. Talari, "Microstructure and hardness properties investigation of Ti and Nb added FeNiAlCuCrTi x Nb y high entropy alloys," *Transactions of Indian Institute of Metals*, vol. 66, no. 4, pp. 309–312, May 2013, doi: 10.1007/s12666-013-0265-7.

[21] W. Y. Tang and J. W. Yeh, "Effect of aluminum content on plasma-nitrided AlxCoCrCuFeNi high-entropy alloys," *Metallurgical and Materials Transactions*, vol. 40, no. 6, pp. 1479–1486, Apr. 2009, doi: 10.1007/s11661-009-9821-5.

[22] C. Li, J. C. Li, M. Zhao, and Q. Jiang, "Effect of alloying elements on microstructure and properties of multiprincipal elements high-entropy alloys," *Journal of Alloys and Compounds*, vol. 475, no. 1–2, pp. 752–757, May 2009, doi: 10.1016/j.jallcom.2008.07.124.

[23] Y. Dong, K. Zhou, Y. Lu, X. Gao, T. Wang, and T. Li, "Effect of vanadium addition on the microstructure and properties of AlCoCrFeNi high entropy alloy," *Materials in Engineering*, vol. 57, pp. 67–72, May 2014, doi: 10.1016/j.matdes.2013.12.048.

[24] G. W. Stachowiak and A. W. Batchelor, *Engineering tribology*, Fourth Edition, Butterworth-Heinemann, 2014, doi: 10.1016/C2011-0-07515-4.

[25] B. Bhushan, *Introduction to Tribology*, Second Edition, Tribology Series, Wiley, 2013, doi: 10.1002/9781118403259.

[26] C. H. Huang, Y. Zhang, R. Vilar, and J. Shen, "Dry sliding wear behavior of laser clad TiVCrAlSi high entropy alloy coatings on Ti-6Al-4V substrate," *Materials in Engineering*, vol. 41, pp. 338–343, Oct. 2012, doi: 10.1016/j.matdes.2012.04.049.

[27] M. Morcillo, B. Chico, J. Alc, and I. D, "SEM / Micro-Raman Characterization of the Morphologies of Marine Atmospheric Corrosion Products Formed on Mild Steel," *Journal of the Electrochemical Society*, vol. 163, no. 8, pp. 426–439, Jan. 2016, doi: 10.1149/2.0411608jes.

[28] G. Deo and I. E. Wachs, "Predicting molecular structures of surface metal oxide species on oxide supports under ambient conditions," *Journal of Physical Chemistry*, vol. 95, no. 15, pp. 5889–5895, Jul. 1991, doi: 10.1021/j100168a033.

[29] V. G. Hadjiev, M. N. Iliev, and I. V. Vergilov, "The Raman spectra of Co_3O_4," *Journal of Physics C: Solid State Physics*, vol. 21, no. 7, pp. 199–201, Mar. 1988, doi: 10.1088/0022-3719/21/7/007.

[30] F. Adar, "Raman spectra of metal oxides," *Spectrosc. (Santa Monica)*, vol. 29, no. 9, Oct. 2014, doi: 10.1007/978-3-030-26803-9-4.

[31] P. F. Mcmillan and A. M. Hofmeister, "Infrared and Raman spectroscopy," *in Spectroscopic Methods in Mineralogy and Geology*, pp. 99–160, 2019, doi: 10.1201/b16932-10.

[32] J. Jehng and I. E. Wachs, "Structural chemistry and raman spectra of niobium oxides," *Chemistry Materials*, vol. 3, no. 1, pp. 100–107, Jan. 1991, doi: 10.1021/cm00013a025.

[33] T. Scharf, S. V. Prasad, P. G. Kotula, J. R. Michael, and C. V. Robino, "Elevated temperature tribology of cobalt and tantalum-based alloys," *Wear*, vol. 330–331, pp. 199–208, 2015, doi: 10.1016/j.wear.2014.12.051.

[34] A. Fu, Z. Xie, W. He, and Y. Cao, "Effect of Temperature on Tribological Behavior of FeCrNi Medium Entropy Alloy," *Metals*, pp. 187–198, no. 2, p. 282, Jan, 2023, doi: 10.3390/met13020282.